ADVANCED FUNCTIONAL MATERIALS
www.afm-journal.de

Regulating Water Adhesion on Superhydrophobic TiO_2 Nanotube Arrays

Ziying Hu, Xuming Zhang, Zhaoyue Liu, Kaifu Huo,* Paul K Chu, Jin Zhai,* and Lei Jiang*

Bioinspired surfaces with special wettability have attracted a significant attention in recent years because of their potential applications for no loss liquid transfer, anti-icing, and self-cleaning. Herein, the realization of two extreme superhydrophobic states on 1H, 1H, 2H, 2H–perfluorooctyltriethoxysilane-modified TiO_2 nanotube arrays (NTAs) is described by changing the structural characteristics of nanotubes while keeping the surface chemical composition constant. The water adhesive force is regulated in a wide range from ≈4.4 to ≈89.6 μN by the nanotubular diameter, length, density, and surface roughness. The cooperation effect between the negative pressures induced by the volume change of sealed air-pockets and the van der Waals' attraction at solid–liquid interface contributes to the water adhesion. The superhydrophobic TiO_2 NTAs with a high adhesive force is used as a "mechanical hand" to transfer water microdroplets without any loss, and the one with extremely low adhesive force is utilized as a self-cleaning and anti-icing surface.

1. Introduction

The design and creation of superhydrophobic surfaces with high water contact angles (CAs) above 150° learning from biological surface have attracted a significant attention in recent years.[1–5] For example, inspired by the micro-/nanostructures in lotus leaves, a superhydrophobic surface with a high CA but a low water adhesive force has been applied for self-cleaning and anti-icing surface.[6–10] On the other hand, inspired by the high adhesive force of gecko's feet to solid surface, superhydrophobic surfaces with a high adhesive force to water are becoming another focus.[2a,11,12] The water droplets can be pinned on the superhydrophobic surfaces at any tilted angles, which contributes to the application for no loss transfer of microdroplets.[13–15]

High adhesive superhydrophobic surfaces have been fabricated by using numerous aligned nanotubes or nanopillars.[12,16] When a water droplet is placed on these surfaces, two kinds of trapped air-pockets exist. One is the sealed air-pockets inside the nanostructures and the other one is the open air-pockets continuous with the atmosphere. The negative pressure induced by the volume change of sealed air-pockets cooperating with van der Waals' attraction contributes to the large water adhesive force.[1d,17,18] Essentially, the water adhesive force on a superhydrophobic surface is determined by its structural characteristics when the surface chemical composition is fixed. Therefore, the control on the surface micro-/nanostructure is capable of regulating the water adhesion on a superhydrophobic surface.[19–22]

The special nanostructure of TiO_2 nanotube arrays (NTAs) formed on the surface of Ti metal by electrochemical anodization are interestingly applied for many technological applications in recent years because of their high photoactivity, robust mechanical property, biological compatibility and chemical stability.[23,24] More importantly, the structural characteristics of TiO_2 NTAs can be controlled facilely by fine design of anodization process.[25,26] Herein, we described the regulation of water adhesion on superhydrophobic TiO_2 NTAs between two extreme wettability states by changing the structural characteristics of nanotubes. The water adhesion force could be regulated over a wide range from 4.4 μN to 89.6 μN by tubular inner diameter (D), length (L), density (ρ) and surface roughness (Rq). It should be mentioned that the switch between these two extreme wettability states has been realized on nanostructured TiO_2 surface with different morphologies (nanopore, nanotube, and nanovesuvianite),[25] which, however, has not yet been realized on the surface of TiO_2 NTAs to the best of our knowledge. The facile adjustability in structural characteristics of TiO_2 NTAs can regulate the water adhesion force in a wide range continuously, which may meet various technological demands. The high adhesive superhydrophobic TiO_2 NTAs were used as a "mechanical hand" to transfer water microdroplets without any loss, and the ones with extremely low adhesive force functioned as a self-cleaning and anti-icing surface. We believed that our

Z. Hu, Prof. Z. Liu, Prof. J. Zhai, Prof. L. Jiang
Key Laboratory of Bio-Inspired Smart Interfacial Science and Technology of Ministry of Education
Beijing Key Laboratory of Bio-inspired Energy Materials and Devices
School of Chemistry and Environment
Beihang University
Beijing 100191, China
E-mail: liuzy@buaa.edu.cn; zhaijin@buaa.edu.cn
Dr. X. Zhang, Prof. K. Huo, Prof. P. K. Chu
Department of Physics and Materials Science
City University of Hong Kong
Tat Chee Avenue, Kowloon, Hong Kong, China
E-mail: kfhuo@hust.edu.cn
Prof. K. Huo
Wuhan National Laboratory for Optoelectronics
Huazhong University of Science and Technology
Wuhan 430074, China

DOI: 10.1002/adfm.201401462

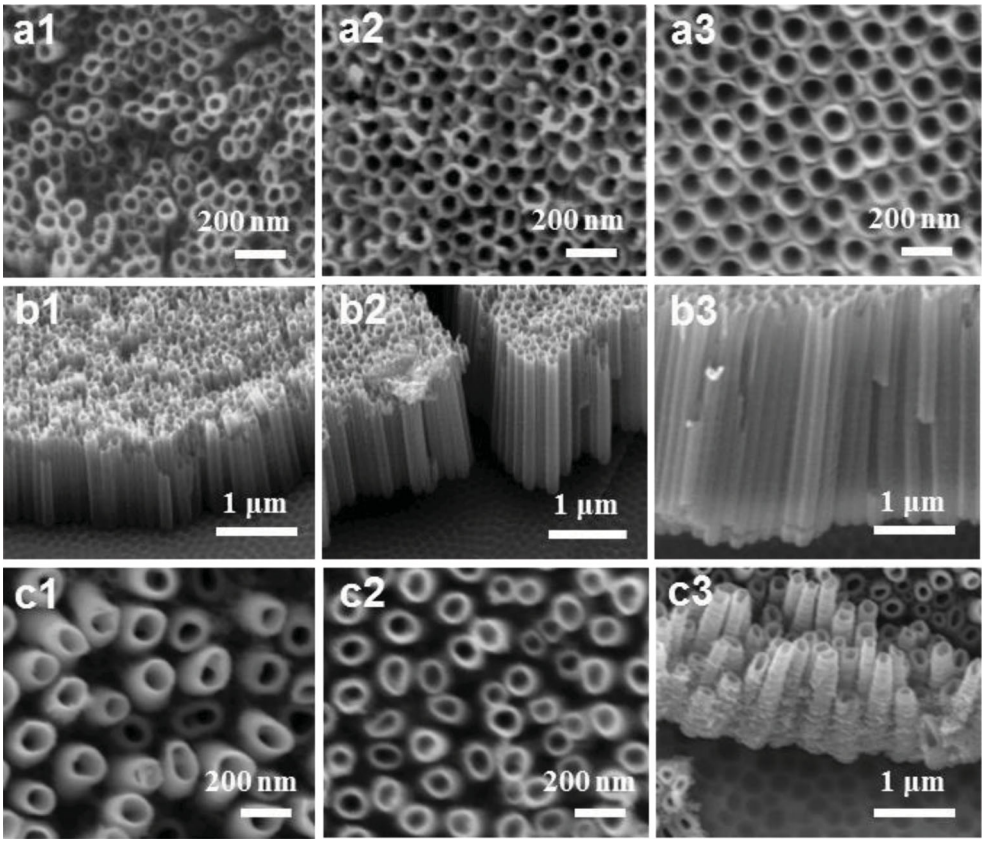

Figure 1. a1–a3) Top-view SEM images of densely arranged TiO_2 NTAs (DA-TiO_2-NTAs) with an inner diameter (D) of ≈29 (a1), ≈68 (a2), and ≈99 nm (a3). The corresponding tubular density (ρ) was calculated to be ≈3.11×10^{10}, ≈1.33×10^{10}, and ≈9.11×10^9 cm^{-2} respectively. The length (L) of nanotubes was ≈1.0 μm. b1–b3) Cross-sectional images of DA-TiO_2-NTAs with L of ≈1.0 (b1), ≈1.4 (b2), and ≈2.8 μm (b3). $D \approx 99$ nm, $\rho \approx 9.11 \times 10^9$ cm^{-2}. c1,c2) Top-view SEM images of non-densely arranged TiO_2 NTAs (NDA-TiO_2-NTAs) with $\rho \approx 2.93 \times 10^9$ cm^{-2} (c1) and ≈7.49×10^9 cm^{-2} (c2). $D \approx 106$ nm. c3) Cross-sectional image of NDA-TiO_2-NTAs with $\rho \approx 2.93 \times 10^9$ cm^{-2}. The fraction of open air-pockets (continuous with the atmosphere) in NDA-TiO_2-NTAs was larger than that in DA-TiO_2-NTAs.

findings might broaden the technical applications of TiO_2 NTAs in more fields, such as no loss liquid transfer, anti-icing surfaces and self-cleaning.

2. Results and Discussion

2.1. Control on the Geometric Parameters of TiO_2 NTAs

The electrochemical anodization of Ti metal in a fluoride-contained organic electrolyte is commonly used to fabricate TiO_2 NTAs on Ti substrate. The anodization parameters including voltage, reaction time and electrolyte determine the structural parameters of nanotubes cooperatively. As shown in **Figure 1**a1–a3, when the electrolyte was 0.3 wt% NH_4F in ethylene glycol containing 5 vol% H_2O, the anodization of Ti foils at 20 V for 4 h, 40 V for 2 h, and 60 V for 30 min produced densely arranged TiO_2 NTAs (DA-TiO_2-NTAs) with inner diameter of ≈29, ≈68, and ≈99 nm respectively. Correspondingly, the wall thickness of nanotubes was about ≈10, ≈12, and ≈19 nm. The length of nanotubes was controlled to be ≈1.0 μm, which was determined by the anodization time at a fixed voltage. The corresponding tubular density was calculated to be ≈3.11×10^{10}, ≈1.33×10^{10}, and ≈9.11×10^9 cm^{-2}. The feature of dense arrangement of nanotubes resulted in very small interspaces between nanotubes. The small tubular diameter at a low voltage is considered to be related with a weak chemical dissolution of TiO_2 by fluoride ions due to the low H^+ concentration. Figure 1b1–b3 shows DA-TiO_2-NTAs with a length of ≈1.0, ≈1.4, and ≈2.8 μm, which were prepared by anodization of Ti metal in the same electrolyte at 60 V for 30 min, 1 h and 2 h respectively. The tubular inner diameter was kept to be ≈99 nm and the corresponding tubular density was ≈9.11×10^9 cm^{-2}. The wall thickness was ≈19 nm. The tubular density could be further lowered by using diethylene glycol electrolyte instead of ethylene glycol electrolyte. As shown in Figure 1c1–c2, when a Ti metal was anodized in a diethylene glycol solution with 2 wt% HF and 3 vol% H_2O at constant voltage of 60 V for 4 h and 8 h, non-densely arranged TiO_2 nanotube arrays (NDA-TiO_2-NTAs) with a low tubular density of ≈7.49×10^9 and ≈2.93×10^9 cm^{-2} were obtained. The wall thickness of nanotubes was about ≈22 and ≈25 nm. The inner diameter of NDA-TiO_2-NTAs was ≈106 nm, which was similar with that of DA-TiO_2-NTAs prepared in an ethylene glycol electrolyte at 60 V for 30 min (Figure 1a3). Because of the similar diameters, the small tubular density in NDA-TiO_2-NTAs resulted in large interspaces between

nanotubes. Interestingly, the lengths of nanotubes in NDA-TiO_2-NTAs with a tubular density of ≈2.93 × 10^9 cm^{-2} (Figure 1c1,c3) were not same, which varied in a range of ≈0.6–1.2 μm (Figure 1c3). The short nanotubes introduced some large holes between long nanotubes, which increased the surface roughness and therefore reduced the fraction of solid–water interface. The significant characteristics of NDA-TiO_2-NTAs were that the fraction of open air-pockets continuous with the atmosphere increased, while the air-pockets in DA-TiO_2-NTAs were mainly sealed in the interior of nanotubes.

2.2. Wettability and Water Adhesion on Superhydrophobic TiO_2 NTAs

The surface of as-prepared TiO_2 NTAs is hydrophilic. To achieve superhydrophobic surfaces, TiO_2 NTAs were modified with 1H, 1H, 2H, 2H-perfluorooctyltriethoxysilane (PTES) molecules.[25,27] The structural parameters of nanotubes including the inner diameter (D), length (L), density (ρ), and surface roughness (Rq) demonstrated a significant role on the surface wettability and water adhesion of PTES-modified TiO_2 NTAs.

Figure 2a shows the CA and adhesive force–distance curve when a water droplet was deposited on the PTES-modified DA-TiO_2-NTAs with a tubular diameter of ≈29 nm and a density of ≈3.11 × 10^{10} (The image was shown in Figure 1a1). The adhesive force was measured using a high-sensitivity micro-electromechanical balance system when a water droplet with a volume of 8 μL gradually approached and retreated from the superhydrophobic surface. The CA of PTES-modified TiO_2 NTAs was ≈151°. For comparison, smooth TiO_2 film was prepared by annealing Ti metal at 450 °C in air for 3 h. The water CA of PTES-modified smooth Ti film is ≈96° (Figure S1, Supporting Information), which indicated that the introduction of nanotubular structure was essential to achieve a superhydrophobic surface. The hydrophobic PTES molecules on the nozzles of TiO_2 NTAs confined the three-phase (gas–liquid–solid) contact lines (TCL), which prevented the intrusion of water into the nanotubes and resulted in trapped air pockets in the interior of nanotubes (sealed air pockets) and in the interspaces between nanotubes (open air pockets). This high fraction of liquid–air contact area contributed to the large CA. Because of the dense arrangement of nanotubes, the air was mainly sealed in the interior of nanotubes by water droplets, which should contribute much to the adhesive force. The maximal water adhesion force on this surface was ≈89.6 μN, which indicated that this surface featured superhydrophobicity with a high water adhesive force. The large adhesive force was caused by the van der Waals' attraction between PTES molecules and water, and the negative pressure induced by the volume change of sealed air-pockets. The high adhesive superhydrophobic TiO_2 NTAs also demonstrated a significant contact angle hysteresis (CAH) of 75.1°, which could be ascribed to the continuous TCL when the water droplet contacted with the surface because of the dense arrangement of TiO_2 NTAs.[28] The water droplet was pinned firmly on the superhydrophobic surface and could resist against its gravitational forces when the surface was tilted vertically (90°) or even turned upside down (180°), indicating that a strong adhesive force existed between the water droplet and the superhydrophobic TiO_2 NTAs (Figure 2b).

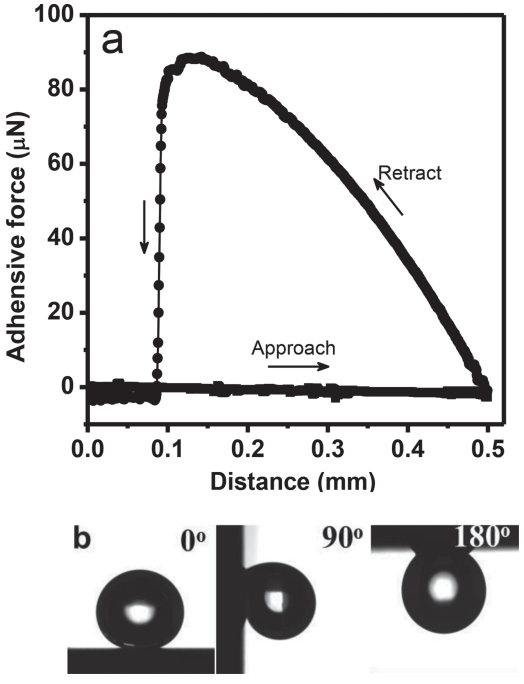

Figure 2. a) The force–distance curve recorded before and after PTES-modified superhydrophobic DA-TiO_2-NTAs contacts with a water droplet. b) The shapes of water droplets on the superhydrophobic DA-TiO_2-NTAs with different tilted angles of 0°, 90°, and 180°. D ≈ 29 nm; L ≈ 1.0 μm; $\rho \approx 3.11 \times 10^{10}$ cm^{-1}. The surface demonstrated a high adhesive superhydrophobicity with a maximal water adhesion force of ≈89.6 μN and a CA of 151 °. The water droplet was pinned firmly on the superhydrophobic surface at a tilted angle of 180 °.

The water adhesive force on the superhydrophobic surface formed by PTES-modified DA-TiO_2-NTAs could be regulated by the inner diameter of individual nanotube when the tubular length was fixed (≈1.0 μm). Because of the dense arrangement of nanotubes, the control of tubular diameter was accompanied by the change of tubular density. **Figure 3** shows the curves of the water CAs and water adhesive forces with respect to the inner diameter nanotubes. When the tubular diameter increased from ≈29 nm up to ≈99 nm, the adhesive force decreased from ≈89.6 to ≈50.6 μN, while the CA increased slightly. Correspondingly, the CAH was decreased from 75.1° to 17.9°, which could be ascribed to the increased tortuosity of TCL by a large tubular diameter.[29] The apparent CA of PTES-modified TiO_2 NTAs can be estimated by equation proposed by Cassie and Baxter:[30]

$$\cos\theta' = f\cos\theta - (1-f) \quad (1)$$

where θ' and θ are the apparent water CAs on a rough and flat TiO_2 surface respectively. The factor f is the fraction of solid–water interface, while $(1 - f)$ is that of the air–water interface. A large tubular diameter resulted in a large fraction of air-water interface $(1 - f)$, which contributed to the slightly increased CAs. The significant decrease of water adhesive force by the increased tubular diameter was ascribed to the following two reasons. One reason was that the increase of

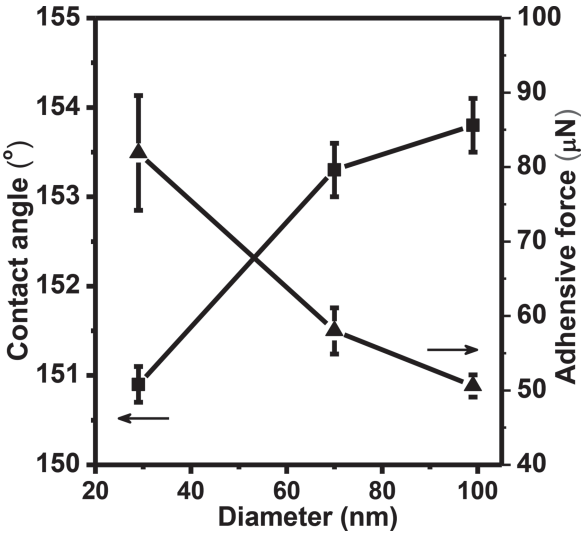

Figure 3. The curves of water CAs and adhesive forces on PTES-modified superhydrophobic DA-TiO_2-NTAs with different diameter D (CA-■, F-▲). $L \approx 1.0$ μm. When D increased, the adhesive force decreased from ≈89.6 to ≈50.6 μN, while the CA increased slightly.

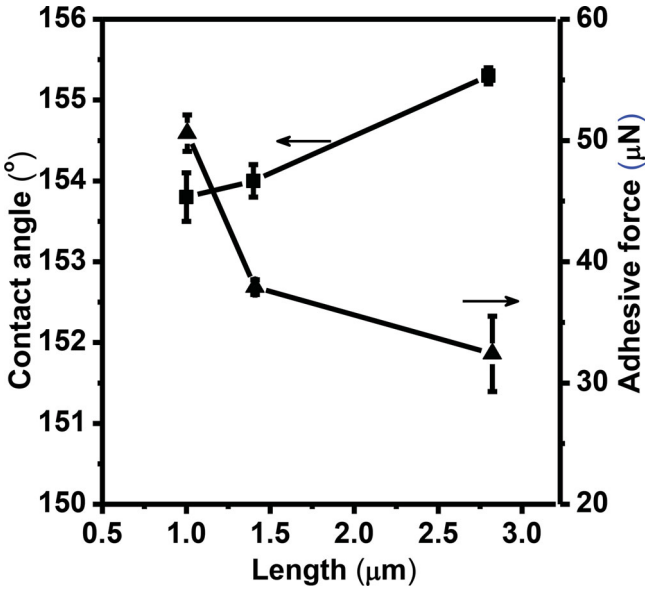

Figure 4. The dependence of water CAs and adhesive force on the length (L) of PTES-modified superhydrophobic DA-TiO_2-NTAs (CA-■, F-▲). $D \approx 99$ nm; $\rho \approx 9.11 \times 10^9$ cm^{-1}. When L increased, the change of CAs was very small, while the adhesive force decreased by 36% from ≈50.6 μN to ≈32.4 μN.

diameter lowered the fraction of solid–water interface, which caused a small van der Waals' attraction between PTES molecules and water. The other one was that the negative pressure (ΔP), which was caused by the volume change of sealed air pockets, decreased following the increase of diameter. The ΔP can be described by the following equation provided that the sealed air was considered to be ideal gas.[25]

$$\Delta P = -\frac{P_0}{(V_0/\Delta V)+1} \quad (2)$$

Here, P_0 and V_0 are the initial pressure and volume of the sealed air pockets. ΔV is the increased volume of sealed air pockets as the water droplet gradually retracted from the superhydrophobic surface. Generally, ΔV is a very small value. Therefore, a large V_0 induced by a large tubular inner diameter would result in a small ΔP, which contributed to the decrement of adhesive force. Note that the adhesive force in our work is larger than that in previous report,[25] which is probably due to the high nanotubular density and the small interspaces between nanotubes in our work.

We investigated the effect of water droplet volume (4, 8, and 16 μL) on the water adhesion forces on PTES-modified DA-TiO_2-NTAs ($D \approx 99$ nm, $\rho \approx 9.11 \times 10^9$ cm^{-2}). As shown in Figure S2 (Supporting Information), when the volume of water droplet used for force measurement was 8 μL, the adhesion force was determined to be ≈50.2 μN. The increase of water droplet volume to be 16 μL did not change the adhesion water obviously (≈52.9 μN). However, a small water droplet with a volume of 4 μL produced a much larger adhesion force of ≈71.6 μN. The water adhesion force was determined by the true contact area between the bottom of the water droplet and the surface of NTAs. If we supposed that the immersing depth of NTAs in water droplet was same, a water droplet with a large curvature radius would result in a large contact area, therefore a large adhesion force. As shown in Figure S3 (Supporting Information), a small water droplet of 4 μL on a metal ring actually had a large curvature radius. The increase of droplet volume to 8 μL decreased the curvature radius due to the deformation of droplet by gravity, which resulted in a small contact area. Further increasing the volume to 16 μL, however, did not change the curvature radius of the bottom of water droplet obviously.

The water adhesive force could further be regulated by the tubular length. **Figure 4** shows the dependence of CAs and adhesion forces on the length of DA-TiO_2-NTAs with constant tubular diameter (≈99 nm) and density (≈9.11×10^9 cm^{-2}). When the tubular length increased from 1.0 to 2.8 μm, the change of CAs was negligible because of the unchanged factor f. The adhesive force, however, decreased by 36% from ≈50.6 μN to ≈32.4 μN. The van der Waals' attraction between PTES molecules and water could be considered to be constant since the tubular diameter and density remained unchanged. It was considered the lowered the negative pressure ΔP induced by the increased tubular length (i.e., large V_0) contributed to the reduction of adhesive force.

The high adhesive superhydrophobic surface could be switched to be a low adhesive state by rationally designing the structural characteristics of TiO_2 NTAs. **Figure 5**a shows the water adhesive forces of PTES-modified non-densely arranged TiO_2 NTAs (NDA-TiO_2-NTAs) with different tubular density. The average inner diameter NTAs were ≈106 nm. The water CAs increased slightly from 151° to 156° following the decrease of tubular density from ≈9.11×10^9 cm^{-2} to ≈2.93×10^9 cm^{-2}, which was explained by the increased fraction of air–water interface. Correspondingly, the adhesive force was lowered from ≈50.6 μN to ≈4.4 μN (Figure 5b) significantly, which switched the superhydrophobic surface from a high adhesive state to be a low adhesive state. The formation of superhydrophobic surface

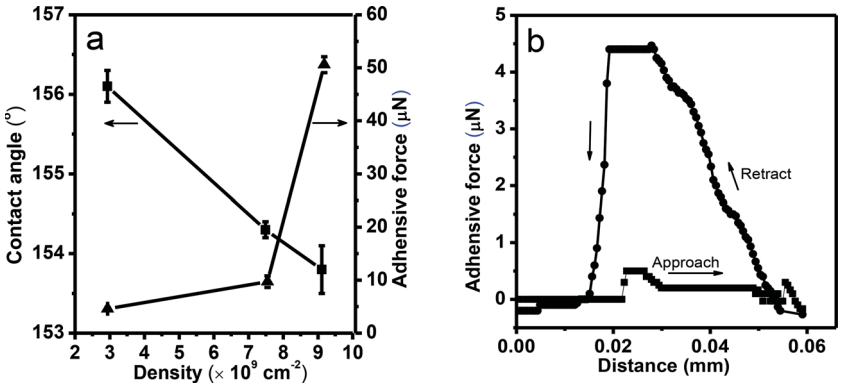

Figure 5. a) The curves of water CAs and adhesive force on the superhydrophobic TiO_2 NTAs with different density (ρ) of nanotubes (CA-■, F-▲). $D \approx 106$ nm. The adhesive force was lowered from ≈50.6 μN to ≈4.4 μN significantly following the decrease of ρ, while the water CAs increased slightly. b) The force–distance curves recorded before and after PTES-modified superhydrophobic NDA-TiO_2-NTAs contact with a water droplet. $D \approx 106$ nm; $\rho \approx 2.93 \times 10^9$ cm^2. The surface demonstrates a superhydrophobicity with an adhesive force of ≈4.4 μN and a CA of 156 °.

with an extremely low water adhesion could be explained by the combination of structural parameters (tubular density and length) and surface roughness. A low tubular density increased the total fraction of air–water interface (including the open and sealed air-pockets). However, the fraction of the sealed air-pockets in the interior of nanotubes was lowered significantly because of the non-dense arrangement. Therefore, when a water droplet gradually retracted from the superhydrophobic surface, the negative pressure ΔP induced by the increased gas volume in the nanotubes was lowered. Furthermore, the lengths of nanotubes in NDA-TiO_2-NTAs (Figure 1c1,c3) with a tubular density of $\approx 2.93 \times 10^9$ cm^{-2} were different, which varied in a range of ≈0.6–1.2 μm. The large holes between long nanotubes induced by the short nanotubes increased the surface roughness. As shown in Figure S4 (Supporting Information), the root mean square roughness (Rq) of NDA-TiO_2-NTAs with a tubualr density of 2.93×10^9 cm^{-2} was ≈85.4 nm determined by the measurements of atomic force microscope (AFM), which was twice as much as that of DA-TiO_2-NTAs with a density of 9.11×10^9 cm^{-2} (Rq = 42.2 nm). The high surface roughness further reduced the fraction of solid–water interface. Therefore, the negative pressure ΔP was reduced significantly. The cooperation between the low negative pressure and small van der Waals' attraction (which was proportional to the fraction of solid–liquid interface) contributed to this extremely low water adhesion. The CAH of low adhesive superhydrophobic TiO_2 NTAs (≈4.4 μN) was measured to be 1.9°, which was ascribed to the very discontinuous TCL by the non-dense arrangement of TiO_2 NTAs and their high surface roughness.[28,29]

2.3. Potential Applications for Microdroplet Transfer, Self-cleaning and Anti-icing

The superhydrophobic TiO_2 NTAs with regulated water adhesion showed some potential technical applications. The high adhesive superhydrophobic TiO_2 NTAs could be used as a "mechanical hand" to transfer a microdroplet with some weight from one surface to another one. As shown in **Figure 6**, when a microdroplet was placed on low adhesive superhydro-phobic TiO_2 NTAs (adhesive force $F \approx 4.4$ μN), high adhesive superhydrophobic TiO_2 NTAs ($F \approx 89.6$ μN) could touch and adhere to this water droplet, which achieved the transfer of the microdroplet between these two extreme surfaces. Furthermore, the water droplet on the high adhesive superhydrophobic surface could be detached to a third surface with a much low CA of ≈96° (PTES-modified smooth Ti film).

Similar with the natural lotus leaves, the superhydrophobic TiO_2 NTAs with an extremely low water adhesion ($F \approx 4.4$ μN) could be used as a self-cleaning surface. The roll of a water droplet removed the dusts on the surface. We used a high-speed camera to record the roll-off behavior of a water droplet. As shown in **Figure 7**, when a water droplet was dropped on the low adhesive superhydrophobic surface, the water droplet rolled off quickly due to the low adhesion force within 0.08 s. When such a surface was contaminated deliberately by chalk dusts, the chalk dusts could be removed by the roll of water droplet, which kept the surface clean automatically.

The regulation of water adhesion on superhydrophobic TiO_2 NTAs also showed technical application for anti-icing (**Figure 8**). We investigated the icing behavior of water droplets (7 μL) on three superhydrophobic surfaces of TiO_2 NTAs with different water adhesion forces of ≈4.4, ≈50.6, and ≈89.6 μN respectively. The humidity and temperature of the environment were controlled to be 66 ± 8% and −7 °C. As shown in Figure 8, at the beginning, these three drops were all transparent on the surfaces. With time going by, they froze and became non-transparent. The delay time (DT) was defined as the time that the water droplet changed from transparent to non-transparent (frozen). The DT of a water droplet on superhydrophobic TiO_2

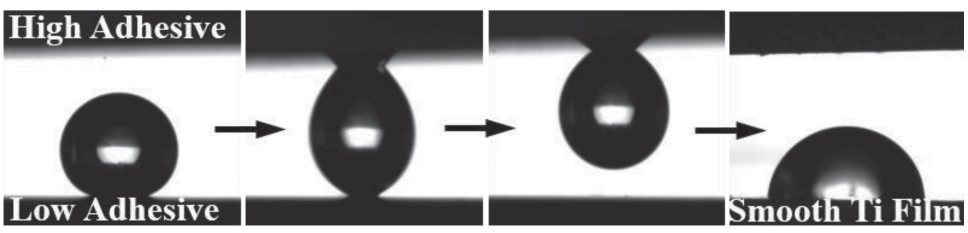

Figure 6. Transfer of a water droplet from low adhesive superhydrophobic TiO_2 NTAs with an adhesive force of ≈4.4 μN to high adhesive superhydrophobic TiO_2 NTAs with an adhesive force of ≈89.6 μN, and then to a third surface with a much low CA of ≈96° (PTES-modified smooth TiO_2 film).

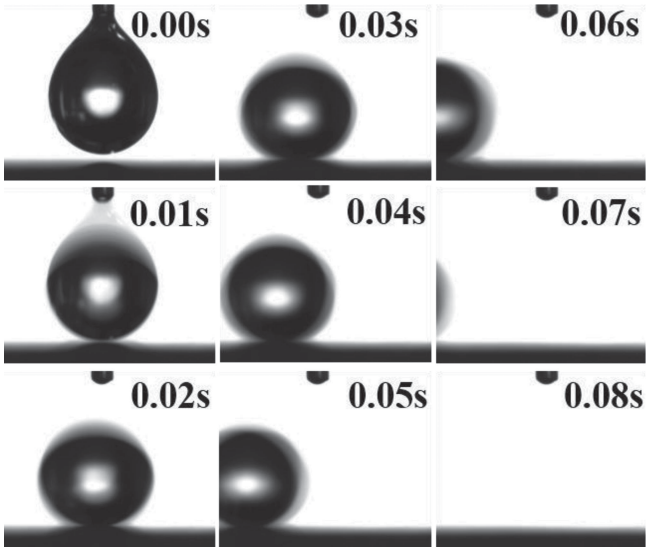

Figure 7. Behavior of a water droplet rolling-off the PTES-modified superhydrophobic NDA-TiO_2-NTAs with extremely low adhesive force of ≈4.4 μN. The time sequence was shown in the top right corners of the images. When a water droplet was placed on the low adhesive superhydrophobic surface, the water droplet rolled off quickly due to the low adhesion force.

NTAs with a high adhesion force of ≈89.6 μN was ≈506 s. The regulation of water adhesion force to be ≈50.6 and ≈4.4 μN increased the DT to be ≈1057 and ≈2829 s. More importantly, during the frozen process of water droplets, the environmental water vapor also showed an icing delay on the low adhesive superhydro-phobic surface. Our results indicated that superhydrophobic TiO_2 NTAs with extremely low adhesive force displayed not only water-repellency but also ice formation delay, which could be acted as potential anti-icing materials.

3. Conclusions

In conclusion, two extreme superhydrophobic states were realized on PTES-modified TiO_2 NTAs by changing the structural characteristics of nanotubes while keeping the surface chemical composition constant. The tubular diameter, length, density and surface roughness demonstrated an essential role on the water adhesion, which regulated the adhesive force in a wide range from ≈4.4 to ≈89.6 μN continuously. The regulated water adhesion was explained by cooperation effect between by the negative pressure induced by the volume change of sealed air-pockets and the van der Waals' attraction at solid–liquid interface. We anticipated that our findings might broaden the applications of TiO_2 NTAs in more fields, such as no-loss liquid transfer, anti-icing, and self-cleaning surfaces.

4. Experimental Section

Fabrication of Superhydrophobic TiO_2 NTAs: TiO_2 NTAs were fabricated by electrochemical anodization in fluoride-contained organic electrolyte.[26,31] In brief, Ti foils (99.7%, Aldrich, 20 × 10 × 1 mm^3) were

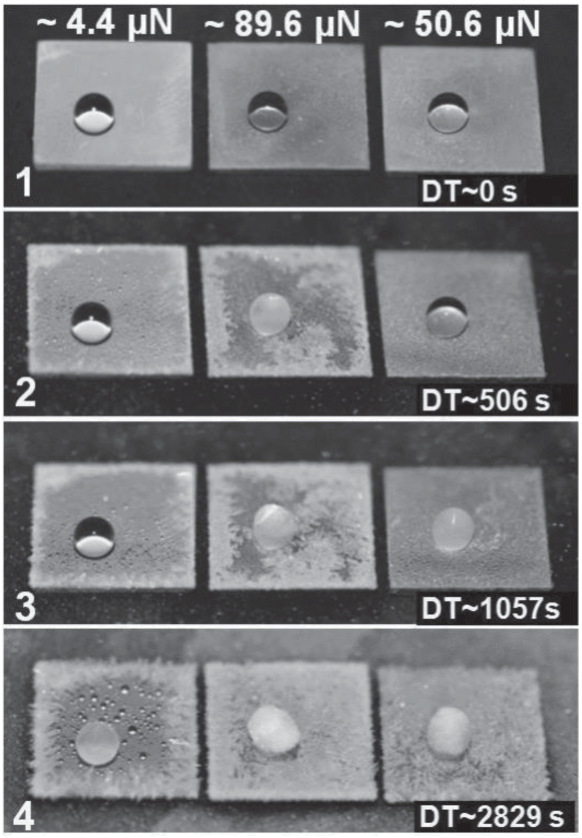

Figure 8. In situ observation of ice formation on three superhydrophobic surfaces of TiO_2 NTAs with water adhesion forces of ≈4.4, ≈50.6, and ≈89.6 μN respectively at −7 °C with delay times (DT). The DT is shown in the bottom right corner of each image. The DT of a water droplet on superhydrophobic TiO_2 NTAs with a high adhesion force of ≈89.6 μN was ≈506 s. The regulation of the water adhesion force to be ≈50.6 and ≈4.4 μN increased the DT to be ≈1057 and ≈2829 s.

firstly polished by SiC sandpapers and then ultrasonically cleaned with acetone (Beijing Chemical Factory), ethanol (Beijing Chemical Factory), and deionized water sequentially. Electrochemical anodization was carried out in a two electrode configuration with a graphite plate cathode and Ti foil anode. After anodization in an ethylene glycol solution with 0.3 wt% NH_4F and 5 vol% H_2O at pulsed voltage (2 s–2 s) of 60 V for 12 h, the first anodized film was removed by ultrasonic cleaning. To prepare densely arranged TiO_2 NTAs (DA-TiO_2-NTAs) with different lengths of ≈1.0, ≈1.4, ≈2.8 μm (D ≈ 99 nm; $\rho \approx 9.11 \times 10^9$ cm^2), the second anodization was carried out at pulsed voltage (2 s–2 s) of 60 V for 30 min, 1 h and 2 h respectively. To fabricate non-densely arranged TiO_2 NTAs (NDA-TiO_2-NTAs) with different inner diameters of ≈29 and ≈68 nm (L ≈ 1.0 μm), the second anodization was under the pulsed voltage (2 s–2 s) of 20 V for 4 h and 40 V for 2 h respectively. To prepare NDA-TiO_2-NTAs with densities of $\approx 7.49 \times 10^9$ and $\approx 2.93 \times 10^9$ cm^2 (D ≈ 106 nm), anodization was done in a diethylene glycol solution with 2 wt% HF and 3 vol% H_2O at constant voltage of 60 V for 4 h and 8 h respectively. These TiO_2 NTAs were rinsed with deionized water and dried under air atmosphere. After annealed at 450 °C under atmosphere for 3 h, TiO_2 NTAs were immersed in a methanolic solution of 1.0 wt% 1H, 1H, 2H, 2H-perfluorooctyltriethoxysilane ($CF_3(CF_2)_5CH_2CH_2Si(OCH_2CH_3)_3$, PTES, Aldrich) for 1 h, and subsequently heated at 140 °C for 1 h.

Characterization: The scanning electron microscopy (SEM) images of TiO_2 nanotube arrays were observed using a field-emission scanning electron microscope (JEOL JSM-7500F, Japan). The surface roughness (Rq) of TiO_2 NTAs was determined by Dimension Icon atomic force

microscope (Bruker). The wettability (static, advancing and receding angle) and adhesive properties of water droplets on the PTES-modified TiO_2 NTAs were characterized using an optical contact-angle meter system (Dataphysics OCA20, Germany). The droplets used for the contact angle (CA) and tilt angle (TA) measurement were 5 μL with a dosing rate of 1 μL s^{-1} at ambient environment with relative humidity about ≈43%. Advancing and receding angles were recorded when water was added to and withdrawn from the water droplet with a syringe respectively. The contact angle hysteresis (CAH) was the difference between advancing and receding angles. The adhesive force was measured using a high-sensitivity micro-electromechanical balance system (Dataphysics DCAT21, Germany). A Water droplet of 8 μL was suspended on a metal ring, and then PTES-modified TiO_2 NTAs were approached and retracted from the water droplet with the sample stage going up and down at a constant speed of 0.01 mm s^{-1} at ambient environment with relative humidity of ≈43%. The NTAs surface started to move down from the droplet once contacted, and the balance force would gradually increase, and reach the maximum before the droplet broke away from the NTAs surface. CAs and adhesive forces were measured at five different locations on each sample, and their average values were reported. Icing delay time (DT) of water droplets on superhydrophobic TiO_2 NTAs was tested by controlling the environmental temperatures down to −7 °C by a Peltier cooling controller with a control precision of 0.5 °C, and observed in situ by the single-lens reflex (SLR) camera. Water drops with the volume of 7 μL were deposited on three superhydrophobic surfaces of TiO_2 NTAs with water adhesion force of ≈4.4 μN, ≈50.6 μN and ≈89.6 μN respectively at the same time. At the beginning, these drops were all transparent on the surfaces, then with time going by, they frozen and became non-transparent. The delay time (DT) was defined as the time that the droplet changed from transparent to non-transparent (frozen). The room temperature was 23 ± 2 °C and the relative humidity was 66 ± 8% controlled by a humidifier.[10a]

Supporting Information

Supporting Information is available from the Wiley Online Library or from the author.

Acknowledgements

Z.H. and X.Z. contributed equally to this work. This work was supported by the National Key Basic Research Program of China (2011CB935704, 2014CB931803), National Natural Science Foundation of China (21003008, 50902104 and 21105077), Beijing Natural Science Foundation (2133066), "Young Talents Plan" for the Universities in Beijing City, Fundamental Research Funds for the Central Universities (YWF-14-HHXY-004) and Scientific Research Foundation for the Returned Overseas Chinese Scholars, State Education Ministry of China. Guangdong – Hong Kong Technology Cooperation Funding Scheme (TCFS) GHP/015/12SZ, and City University of Hong Kong Applied Research Grant (ARG) 9667069. The authors thank Prof. Yongmei Zheng's group in Beihang University for the use of anti-icing instruments.

Received: May 6, 2014
Published online: August 19, 2014

[1] a) X. Yao, Y. L. Song, L. Jiang, *Adv. Mater.* **2011**, *23*, 719; b) X. Feng, L. Jiang, *Adv. Mater.* **2006**, *18*, 3063; c) M. Liu, Y. Zheng, J. Zhai, L. Jiang, *Acc. Chem. Res.* **2010**, *43*, 368; d) S. Wang, L. Jiang, *Adv. Mater.* **2007**, *19*, 3423.

[2] a) K. Autumn, Y. A. Liang, S. T. Hsieh, W. Zesch, W. P. Chan, T. W. Kenny, R. Fearing, R. J. Full, *Nature* **2000**, *405*, 681; b) A. K. Geim, S. V. Dubonos, I. V. Grigorieva1, K. S. Novoselov, A. A. Zhukov, S. Yu. Shapoval, *Nat. Mater.* **2003**, *2*, 461.

[3] a) L. Feng, S. H. Li, Y. S. Li, H. J. Li, L. J. Zhang, J. Zhai, Y. L. Song, B. Q. Liu, L. Jiang, D. B. Zhu, *Adv. Mater.* **2002**, *14*, 1857; b) T. S. Wong, S. H. Kang, S. K. Y. Tang, E. J. Smythe, B. D. Hatton, A. Grinthal, J. Aizenberg, *Nature* **2011**, *477*, 443.

[4] L. Feng, Y. Zhang, J. Xi, Y. Zhu, N. Wang, F. Xia, L. Jiang, *Langmuir* **2008**, *24*, 4114.

[5] X. Liu, Y. Liang, F. Zhou, W. Liu, *Soft Matter* **2012**, *8*, 2070.

[6] M. Jin, X. Feng, J. Xi, J. Zhai, K. Cho, L. Feng, L. Jiang, *Macromol. Rapid Commun.* **2005**, *26*, 1805.

[7] a) L. Jiang, Y. Zhao, J. Zhai, *Angew. Chem. Int. Ed.* **2004**, *116*, 4438; b) R. Blossey, *Nature Mater.* **2003**, *2*, 301; c) X. Zhang, Z. Li, K. Liu, L. Jiang, *Adv. Funct. Mater.* **2013**, *23*, 2881.

[8] J. M. Xi, L. Jiang, *Ind. Eng. Chem. Res.* **2008**, *47*, 6354.

[9] T. Maitra, M. K. Tiwari, C. Antonini, P. Schoch, S. Jung, P. Eberle, D. Poulikakos, *Nano Lett.* **2014**, *14*, 172.

[10] a) P. Guo, Y. Zheng, M. Wen, C. Song, Y. Lin, L. Jiang, *Adv. Mater.* **2012**, *24*, 2642; b) Q. Zhang, M. He, J. Chen, J. Wang, Y. Song, L. Jiang, *Chem. Commun.* **2013**, *49*, 4516.

[11] K. Autumn, M. Sitti, Y. C. A. Liang, A. M. Peattie, W. R. Hansen, S. Sponberg, T. W. Kenny, R. Fearing, J. N. Israelachvili, R. J. Full, *Proc. Natl. Acad. Sci. U.S.A.* **2002**, *99*, 12252.

[12] a) M. H. Jin, X. J. Feng, L. Feng, T. L. Sun, J. Zhai, T. J. Li, L. Jiang, *Adv. Mater.* **2005**, *17*, 1977; b) W. K. Cho, I. S. Choi, *Adv. Funct. Mater.* **2008**, *18*, 1089; c) M. Liu, L. Jiang, *Adv. Funct. Mater.* **2010**, *20*, 3753.

[13] a) M. Wang, C. Chen, J. Ma, J. Xu, *J. Mater. Chem.* **2011**, *21*, 6962; b) L. Feng, Y. Zhang, J. Xi, Y. Zhu, N. Wang, F. Xia, L. Jiang, *Langmuir* **2008**, *24*, 4114.

[14] X. Q. Zhang, S. H. Wan, J. B. Pu, L. P. Wang, X. Q. Liu, *J. Mater. Chem.* **2011**, *21*, 12251.

[15] A. Winkleman, G. Gotesman, A. Yoffe, R. Naaman, *Nano Lett.* **2008**, *8*, 1241.

[16] K. S. Liu, J. X. Du, J. T. Wu, L. Jiang, *Nanoscale* **2012**, *4*, 768.

[17] X. D. Zhao, H. M. Fan, J. Luo, J. Ding, X. Y. Liu, B. S. Zou, Y. P. Feng, *Adv. Funct. Mater.* **2011**, *21*, 184.

[18] J. Yong, F. Chen, Q. Yang, D. S. Zhang, H. Bian, G. Q. Du, J. H. Si, X. W. Meng, X. Hou, *Langmuir* **2013**, *29*, 3274.

[19] J. Li, X. Liu, Y. Ye, H. Zhou, J. Chen, *J. Phys. Chem. C* **2011**, *115*, 4726.

[20] B. Bhushan, K. Koch, Y. C. Jung, *Soft Matter* **2008**, *4*, 1799.

[21] X. J. Huang, D. H. Kim, M. Im, J. H. Lee, J. B. Yoon, Y. K. Choi, *Small* **2009**, *5*, 90.

[22] N. Zhao, Q. D. Xie, X. Kuang, S. Q. Wang, Y. F. Li, X. Y. Lu, S. X. Tan, J. Shen, X. L. Zhang, Y. J. Zhang, J. Xu, C. C. Han, *Adv. Funct. Mater.* **2007**, *17*, 2739.

[23] a) G. K. Mor, O. K. Varghese, M. Paulose, K. Shankar, C. A. Grimes, *Sol. Energy Mater. Sol. Cells* **2006**, *90*, 2011; b) K. Shankar, J. I. Basham, N. K. Allam, O. K. Varghese, G. K. Mor, X. Feng, M. Paulose, J. A. Seabold, K. Choi, C. A. Grimes, *J. Phys. Chem. C* **2009**, *113*, 6327.

[24] a) K. Lee, D. Kim, P. Roy, I. Paramasivam, B. I. Birajdar, E. Spiecker, P. Schmuki, *J. Am. Chem. Soc.* **2010**, *132*, 1478; b) Y. Song, F. S. Stein, S. Bauer, P. Schmuki, *J. Am. Chem. Soc.* **2009**, *131*, 4230.

[25] Y. Lai, X. Gao, H. Zhuang, J. Huang, C. Lin, L. Jiang, *Adv. Mater.* **2009**, *21*, 3799.

[26] a) S. Yoriya, G. K. Mor, S. Sharma, C. A. Grimes, *J. Mater. Chem.* **2008**, *18*, 3332; b) E. Balaur, J. M. Macak, H. Tsuchiya, P. Schmuki, *J. Mater. Chem.* **2005**, *15*, 4488; c) E. Balaur, J. M. Macak, L. Taveira, P. Schmuki, *Electrochem. Commun.* **2005**, *7*, 1066.

[27] Y. K. Lai, C. J. Lin, J. Y. Huang, H. F. Zhuang, L. Sun, T. Nguyen, *Langmuir* **2008**, *24*, 3867.

[28] W. Chen, A. Y. Fadeev, M. C. Hsieh, D. Öner, J. Youngblood, T. J. McCarthy, *Langmuir* **1999**, *15*, 3395.

[29] D. Öner, T. J. McCarthy, *Langmuir* **2000**, *16*, 7777.

[30] a) A. B. D. Cassie, S. Baxter, *Trans. Faraday Soc.* **1944**, *40*, 546; b) Z. Cheng, J. Gao, L. Jiang, *Langmuir* **2010**, *26*, 8233; c) Z. J. Cheng, L. Feng, L. Jiang, *Adv. Funct. Mater.* **2008**, *18*, 3219.
[31] a) J. Park, S. Bauer, K. von der Mark, P. Schmuki, *Nano Lett.* **2007**, *7*, 1686; b) C. A. Grimes, *J. Mater. Chem.* **2007**, *17*, 1451; c) Z. Liu, Z. Hu, H. Huang, Q. Zhang, T. Zhang, J. Zhai, L. Jiang, *J. Mater. Chem.* **2012**, *22*, 22120; d) J. M. Macak, P. Schmuki, *Electrochim. Acta* **2006**, *52*, 1258; e) P. Roy, S. Berger, P. Schmuki, *Angew. Chem. Int. Ed.* **2011**, *50*, 2904; f) H. E. Prakasam, K. Shankar, M. Paulose, O. K. Varghese, C. A. Grimes, *J. Phys. Chem. C* **2007**, *111*, 7235; g) Z. Liu, Q. Zhang, T. Zhao, J. Zhai, L. Jiang, *J. Mater. Chem.* **2011**, *21*, 10354.